Stable and Bright Electroluminescent Devices Utilizing Emissive 0D Perovskite Nanocrystals Incorporated in a 3D $CsPbBr_3$ Matrix

*Aditya Mishra, Riya Bose, Yangzi Zheng, Weijie Xu, Reema McMullen, Abhas B. Mehta, Moon J. Kim, Julia W. P. Hsu, Anton V. Malko, and Jason D. Slinker**

Dr. A. Mishra, W. Xu, A. B. Mehta, Prof. M. J. Kim, Prof. J. W. P. Hsu, Prof. J. D. Slinker
Department of Materials Science and Engineering
The University of Texas at Dallas
800 West Campbell Rd.
Richardson, Texas 75080-3021, United States.
E-mail: slinker@utdallas.edu

Dr. R. Bose, Y. Zheng, Dr. R. McMullen, Prof. A. V. Malko, and Prof. J. D. Slinker
Department of Physics
The University of Texas at Dallas
800 West Campbell Rd.
Richardson, Texas 75080-3021, United States.

Prof. J. D. Slinker
Department of Chemistry
The University of Texas at Dallas
800 West Campbell Rd.
Richardson, Texas 75080-3021, United States.

Aditya Mishra and Riya Bose contributed equally to this work.

Keywords: 0D-3D composite, PeLEC, electroluminescence, perovskites, Cs_4PbBr_6 nanocrystals

The zero-dimensional (0D) cesium lead halide perovskite Cs_4PbBr_6 has drawn remarkable interest due to its highly efficient robust green emission compared to its three-dimensional (3D) $CsPbBr_3$ counterpart. However, seizing the advantages of the superior photoluminescence properties for practical light-emitting devices remains elusive. To date, Cs_4PbBr_6 has been employed only as a higher-bandgap non-luminescent matrix to passivate or provide quantum/dielectric confinement to $CsPbBr_3$ in light-emitting devices and to enhance its photo/thermal/environmental stability. To resolve this disparity, we designed a novel solvent engineering method to incorporate highly luminescent 0D Cs_4PbBr_6 nanocrystals (PNCs) into a 3D $CsPbBr_3$ film, forming the active emissive layer in single-layer perovskite light-emitting electrochemical cells (PeLECs). We observed a dramatic increase of the maximum external quantum efficiency (EQE) and luminance from 2.7% and 6050 cd m^{-2} for a 3D-only PeLEC to 8.3% and 11200 cd m^{-2} for a 3D-0D PNC device with only 7% by weight of 0D PNCs. The majority of this increase is driven by efficient inherent emission of 0D PNCs, while the concomitant morphology improvement also contributes to reduced leakage current, reduced hysteresis, and enhanced operational lifetime (half-life of 129 h), making this one of the best performing LECs reported to date.

1. Introduction

In recent years, lead halide perovskites have been the community's choice material, exhibiting high absorption coefficients, long carrier diffusion lengths, and defect tolerance, leading to skyrocketing performance in thin-film optoelectronics.[1] Compared to hybrid organic-inorganic perovskites, inorganic perovskites offer improved chemical and thermal stability while retaining most of the advantageous properties. In particular, cesium lead halide perovskites ($CsPbX_3$, X= Cl, Br, I) have gained significant attention for light-emitting applications because of their high photoluminescence (PL) quantum yield (QY), color-purity, widely tunable emission, and facile solution processability.[2] Recently, green perovskite LEDs have achieved impressive external quantum efficiencies (EQE) approaching and exceeding ~20%.[3] However, $CsPbX_3$ light-emitting devices still suffer from fast excitonic decay due to weakly bound excitons that can be easily thermally dissociated and diffused with lattice vibration, thereby being trapped by non-radiative defect states, which arise due to their labile surface as well as environmental factors.[4] This rapid excitonic decay renders the PLQY sensitive to the material form and requires additional defect passivation/encapsulation strategies such as embedding in polymer additives, incorporating dopants, and engineering ligand shells to circumvent this issue.[4a, 5]

Contrary to the 3D perovskites $CsPbX_3$, where the $[PbX_6]^{4-}$ octahedra are corner shared along all three dimensions, isolation of octahedra in 0D Cs_4PbX_6 leads to a higher exciton binding energy and, consequently, a remarkable enhancement of PL intensity that remains in the solid-state along with superior environmental stability.[6] The origin of the emission in 0D perovskites, which spectrally is nearly identical to the 3D perovskites despite the higher bandgap of the former, has often been assigned to the embedded 3D impurities.[7] However, several studies have ruled out the presence of 3D impurities by intensive structural characterization and attributed the origin of the emission to the presence of molecular-like intra-

bandgap defects.[6a, 8] In particular, 0D Cs_4PbBr_6 has been extensively studied from both theoretical and experimental aspects, and it has been observed that Br vacancies (V_{Br}) in 0D Cs_4PbBr_6 have a low formation energy and can induce a mid-gap energy level appropriate to achieve the green emission.[9] Thus, there is considerable literature evidence demonstrating emission from 0D Cs_4PbBr_6 (Table S1, Supporting Information).[6a, 8-9] Notably, non-emissive Cs_4PbBr_6 has found widespread application as a matrix to encapsulate $CsPbBr_3$, as it can passivate the surface by endotaxy without any resulting strain.[10] Such a non-luminescent 0D phase restricts the growth of $CsPbBr_3$ crystallites, leading to increased confinement and enhancement of exciton binding energy.[11] Cs_4PbBr_6, being a higher bandgap material, can also provide type-I confinement to $CsPbBr_3$, thereby restricting the carriers within the $CsPbBr_3$ region and reducing the probability of electron leakage,[12] or can provide dielectric confinement to the 3D part, enhancing its oscillator strength and absorption cross-section.[13] Energy transfer from the 0D to 3D has also been reported.[14] Overall, reducing non-radiative losses and facilitating radiative recombination significantly enhance the EQE of $CsPbBr_3$ light-emitting devices. Additionally, it also improves the photo, thermal, and environmental stability of the devices, resulting in longer operational lifetimes.[11b, 15]

Surprisingly, regardless of all the efforts to identify the origin of the emission, much less has been done to implement its propitious emission properties in light-emitting devices, with limited reports of using them for luminescent solar concentrators, white LEDs, lasing, and X-ray scintillators.[16] Here, we designed a novel solvent engineering method to incorporate highly emissive 0D perovskite nanocrystals (PNCs) into a 3D perovskite composite film ($CsPbBr_3$, a polyelectrolyte, and Li salt) to form the emissive layer in single-layer perovskite light-emitting electrochemical cells (PeLEC).[17] Light-emitting electrochemical cells utilize mobile ion redistribution to enhance charge injection and produce efficient emission from solution processible single-layer devices.[18] It is observed that incorporation of an optimized concentration of highly luminescent (PLQY ~70%) 0D PNCs in a $CsPbBr_3$ matrix can

dramatically improve virtually all of the PeLEC optoelectronic properties. In particular, PeLECs utilizing these highly emissive 0D PNCs exhibit a maximum luminance of 11200 cd m^{-2}, a maximum power efficiency of 33.0 Lm W^{-1}, a maximum external quantum efficiency of 8.3%, and a long luminescence half-life of 129 h when operated at 10 mA cm^{-2}. The rationale for this enhancement is established by a detailed analysis of the photoluminescence and electroluminescence of various film and device formulations coupled with morphological and structural evaluation by microscopy and diffraction.

2. Results and Discussion

2. 1. Fabrication and PL of 3D-0D Blended Films

Figure 1a presents our method to fabricate 3D-0D PNC light-emitting electrochemical cells. Since the morphology of the film is a crucial component to ensure optimum device performance, our major challenge was to distribute the 0D PNCs into the 3D matrix while retaining its crystal structure network. To achieve this, we modified our previously reported procedure used to fabricate standard 3D perovskite light-emitting electrochemical cell. Typically, a precursor solution of the 3D $CsPbBr_3$ ($CsBr:PbBr_2$, mixing ratio of 1.5:1), poly(ethylene oxide) electrolyte, and $LiPF_6$ salt additive was spin-cast from DMSO solution onto glass slides bearing the modified bottom electrode of ITO/PEDOT-PSS. Selective addition of polyelectrolyte and salt of highly mobile ions is advantageous to attain differentiated ion motion in PeLECs and maintaining perovskite ionic crystal,[17c, 17e, 17f] as illustrated in Figure 1b. Once this film was set, pre-synthesized 0D Cs_4PbBr_6 PNCs (synthesized following literature reported procedure[9c]) in different weight ratios were introduced utilizing a hydrofluoroether (HFE) "orthogonal solvent," a solvent that selectively suspends the 0D PNCs while maintaining the underlying structure of the film (Figure S1 and Table S2, Supporting Information).[19]

(Notably, the long-chain ligands present on 0D PNCs prohibited using them as the sole emitters in PeLECs.) The utility of HFEs to nondestructively interact with 3D perovskite films has been previously established.[19b] Afterwards, the film was annealed in vacuum and at 150 °C to set the crystal structure of the film.

Figure 1c shows the steady state absorption (inset) and emission spectra of the individual 3D, 0D PNCs (70% PLQY) and the 3D-0D PNCs composite films. While the absorption spectrum of the composite shows collective features of both 3D and 0D, the emission spectrum reveals an emission peak of similar FWHM centered at 523 nm, which is slightly blue-shifted compared to 3D (~525 nm) and 0D (~524 nm) components. However, the PL lifetime (Figure 1d) of the composite emission is significantly elongated compared to either 3D or 0D films, implying reduction of fast carrier trapping channels.

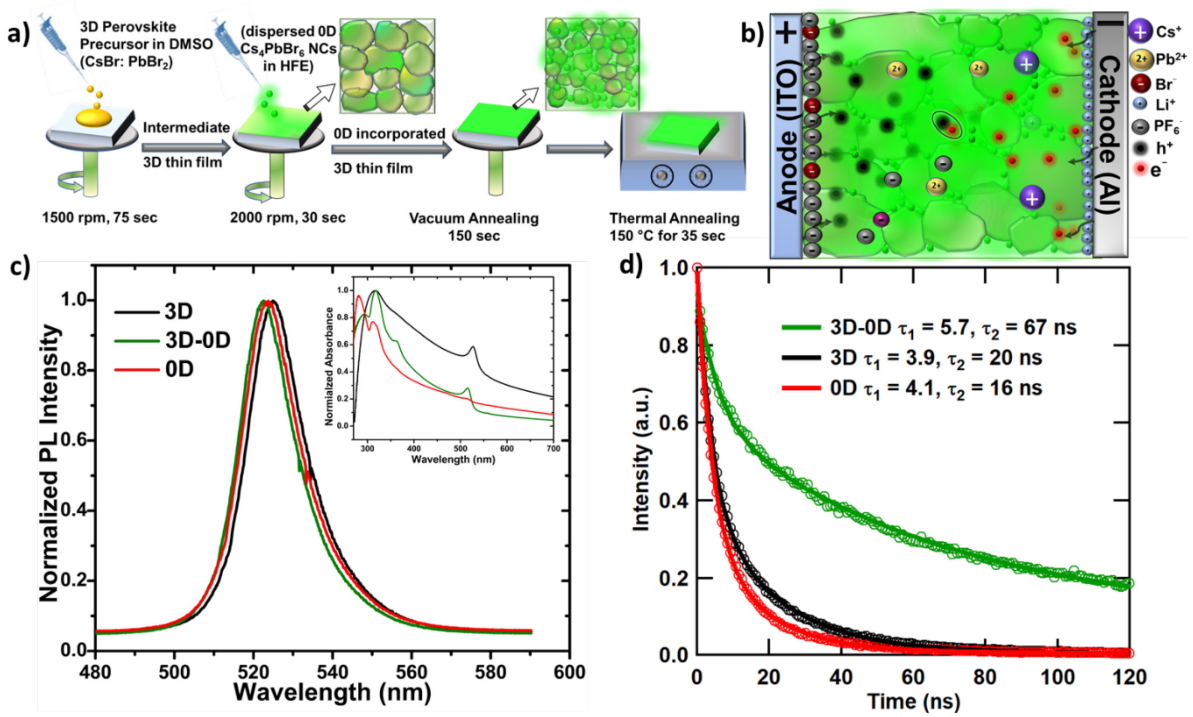

Figure 1. Fabrication method and photoluminescence (PL) from thin films of 0D and 3D perovskite blends. a) Illustration of the fabrication method for dispersing 0D PNCs in a 3D matrix. b) Illustration of the ionic redistribution and charge dynamics in PeLECs. c) Normalized steady-state PL spectra of 0D, 3D, and 3D-0D perovskite composite thin films. (Inset: Absorbance spectra of 0D, 3D, and 3D-0D perovskite composite thin films.) d) Normalized time-resolved PL spectra of 0D, 3D, and 3D-0D perovskite composite thin films.

2.2 3D-0D PNC PeLECs

Since the 3D-0D PNCs blend showed a clear improvement of the PL properties over the 3D counterpart, we compared their electroluminescence performance as the active material in PeLECs with an ITO/PEDOT-PSS/perovskite:PEO:$LiPF_6$/LiF/Al architecture. To further investigate how the intrinsic PL qualities of 0D PNCs affect the overall emission from the composite device, we employed emissive 0D PNCs with high (~70%) and low (~30%) PLQY, as well as non-emissive 0D PNCs synthesized per literature-reported procedures.[7b,9d] **Figure 2**a shows the electroluminescence (EL) spectra of 3D and 3D-0D PNCs PeLECs with 0D PNCs of various PLQY under 4.5 V bias. The 3D films exhibit a narrow EL emission peak centered at 522 nm, characteristic of $CsPbBr_3$ PeLECs,[17b-d] whereas 3D-0D PNCs composites exhibited slightly blue-shifted emission centered at 518 nm, similar to the blueshift observed in the PL. EL spectra featuring similar characteristics as PL indicate a minimal impact of the fabrication process on the integrity of the perovskite thin film. However, the EL intensities of the composites with emissive 0D PNCs are significantly higher than that of the 3D-only device, with the high PLQY composite producing an approximately 3-fold enhancement of the maximum. By contrast, the 3D-0D composite with non-emissive 0D PNCs has a lower EL intensity than the 3D-only device.

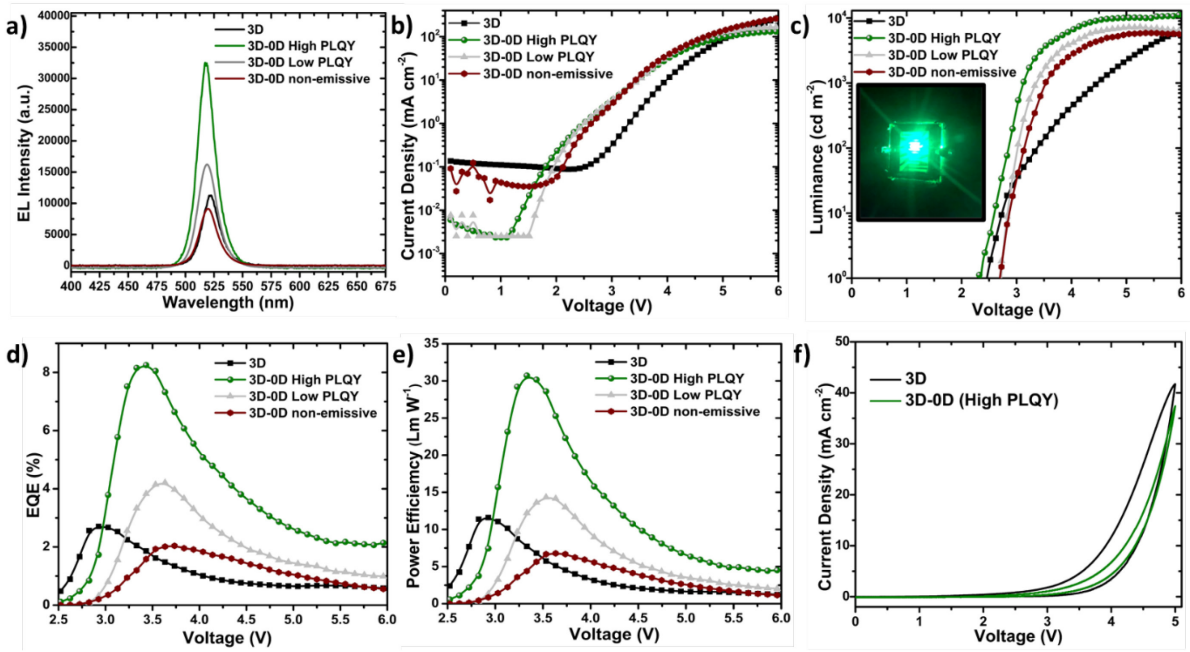

Figure 2. Electroluminescence spectra and luminance-current-voltage characteristics of 3D and 3D-0D PeLECs. a) Electroluminescence spectra of 3D and 3D-0D PeLECs at 4.5 V. b) Current density versus voltage for 3D and 3D-0D PeLECs. c) Luminance versus voltage for 3D and 3D-0D PeLECs. (Inset: Operation of a 3D-0D (high PLQY) PeLEC at 4.5 V.) d) EQE versus voltage for 3D and 3D-0D PeLECs. e) Power efficiency versus voltage for 3D and 3D-0D PeLECs. f) Current density versus voltage sweeps for 3D and 3D-0D PeLECs.

The current densities of the 3D and 3D-0D PeLECs from current/voltage sweeping from 0 to 6V are presented in Figure 2b. The redistribution of ions largely dictates current injection in single layer LECs, and the thin film quality governs background/leakage current. The 3D device exhibits significant leakage current (~0.1 mA/cm^2) at low voltages and an onset of significant current injection above this threshold near 2.8 V. Adding the 0D PNCs lowers the leakage current density, with the 3D-0D (low PLQY) PeLEC and the 3D-0D (high PLQY) decreasing leakage current by an order of magnitude. Furthermore, the onset of current injection above this threshold is lowered to 2.0 V for the 3D-0D (non-emissive) PeLEC, 1.6 V for the 3D-0D (low PLQY) PeLEC, and 1.3 V for the 3D-0D (high PLQY). This lowered injection voltage threshold suggests that the 0D PNCs help facilitate ionic transport, potentially through the passivation of trapping channels from the 3D perovskite lattice, as evidenced from time-resolved PL.

Figure 2c shows the luminance of the PeLECs from current/voltage sweeping from 0 to 6V. The onset of luminance above 1 cd m^{-2}, characteristic of the injection of the minority carrier, is observed between 2.3-2.7 V for these devices, with the 3D-0D (high PLQY) sample possessing the lowest onset voltage threshold. Likewise, the voltage to surpass 100 cd m^{-2} luminance lowers from 3.4 V for the 3D-only PeLEC to 2.9 V for the 3D-0D (high PLQY) device. Over this 6 V range, the 3D device peaks at a luminance of 6050 cd m^{-2}, the 3D-0D (non-emissive) PeLEC at 5800 cd m^{-2}, the 3D-0D (low PLQY) PeLEC at 7300 cd m^{-2}, and the 3D-0D (high PLQY) at 11200 cd m^{-2}. (See Figure S2, Supporting Information, for a statistical comparison of luminance maxima.) Thus, incorporating either low or high PLQY 0D PNCs to 3D film leads to higher peak luminance, whereas the non-emissive 0D lowers peak luminance. In addition, while the low PLQY 0D insertion improves this metric by only ~20%, the high PLQY 0D PNCs raise the luminance by 85%. This differential enhancement unequivocally indicates that the intrinsic emission quality of the 0D PNCs is the prime factor enhancing the luminance of the composite PeLECs.

To further understand how 0D PNCs impact PeLEC performance, the efficiency metrics from these devices are shown in Figure 2d and 2e. The external quantum efficiency (EQE) of the 3D-only PeLEC peaks at 2.7% photons/electron, as seen in Figure 2d. The addition of the low PLQY 0D PNCs raises this peak EQE to 4.2%, while the high PLQY device maximizes at 8.3%, among the best values reported for single-layer LECs.[20] Alternatively, the 3D-0D (non-emissive) PeLEC decreases the peak EQE to 2.0%, and likewise decreases other efficiency metrics (Table S2, Supporting Information). (See Figure S2, Supporting Information, for a statistical comparison of EQE maxima.) The power efficiency maximum improves from 11.6 lm W^{-1} for the 3D-only PeLEC to 14.3 lm W^{-1} for the 3D-0D (low PLQY) PeLEC, to 33.0 lm W^{-1} for the 3D-0D (high PLQY) PeLEC. Again, this 33.0 lm W^{-1} measure is among the best reported for single-layer LECs.[20] What is more, these efficiency metrics are achieved at 3070 cd m^{-2} for the 3D-0D (high PLQY) PeLEC. Thus, the inclusion of emissive 0D PNCs into a 3D

perovskite matrix greatly enhances quantum and power efficiency metrics, with the 3D-0D (high PLQY) PeLEC rivaling the best performance in the field for single layer LECs. Furthermore, while the low PLQY 0D PNCs improve the efficiency over 3D-only devices by ~25-55%, introducing the high PLQY 0D PNCs into the film doubles and triples the EQE and power efficiency, respectively. Again, these metrics demonstrate that the efficiency of the 0D PNC emission determines the efficiency of 3D-0D blended PeLECs.

In addition, blending the 0D PNCs into the 3D matrix reduces the hysteresis associated with cyclic PeLEC operation. Hysteresis in LECs occurs from slow ion relaxation. Figure 2f shows the plot from cyclic current-voltage sweeping of 3D and 3D-0D high PLQY PeLECs. The hysteresis in current is greatly reduced, indicating more efficient ion transport with the inclusion of the 0D PNCs.

To assess the impact of emissive 0D PNCs on the stability of the PeLECs, the devices were operated at constant current, with the data presented in **Figure 3**a and 3b. One general metric is the luminance half-life, the time to decay from the maximum to half maximum. Under 33.3 mA cm^{-2} operation, the 3D PeLEC achieves a 3120 cd m^{-2} luminance maximum and exhibits a luminance half-life of 26.0 h. Likewise, under 33.3 mA cm^{-2} operation, the 3D-0D (high PLQY) PeLEC achieves a 3640 cd m^{-2} luminance maximum and exhibits a luminance half-life of 46.2 h, highly competitive among PeLEC devices (Table S3, Supporting Information). As lifetimes of PeLECs generally scale inversely with luminance as a power law we also ran the 3D-0D (high PLQY) PeLEC at a constant current density of 10 mA cm^{-2} to observe longer lifetimes. For this experiment, the PeLEC peaked at a luminance maximum of 1530 cd m^{-2} and yielded a half-life of 129 h, among the best for perovskite light-emitting devices (Table S3, Supporting Information).[3a, 5i, 17c, 21] This lifetime enhancement is likely owed to the passivation of the 3D perovskite matrix by stable and emissive 0D PNCs and the preservation of the perovskite lattice by differentiated ion motion in the PeLEC—selective redistribution of the $LiPF_6$ additive ions.

In Figure 3b, the operational voltage for each device under constant current is plotted. Constant current generally induces a higher voltage in the initial stages of operation while the device is resistive, encouraging facile ionic redistribution. On longer timescales, the voltage lowers as ion accumulation at the electrodes increases charge injection and lowers device resistance. For the 3D PeLEC at 33.3 mA cm^{-2} constant current, after beginning near 4 V, the steady-state voltage ranges from 3.0 to 3.4 V. The 3D-0D PeLEC at 33.3 mA cm^{-2} also initiates near 4V, but the voltage quickly lowers to operate at a low 2.5-2.7 V. This suggests that the 0D PNCs improve the conductivity of the overall device, and, given the observations from I-V testing, this improvement may originate from more facile ionic redistribution enhancing injection and carrier density. At 10.0 mA cm^{-2}, the 3D-0D PeLEC achieves an even lower steady-state voltage of 2.3 V, approaching the bandgap of these perovskites.

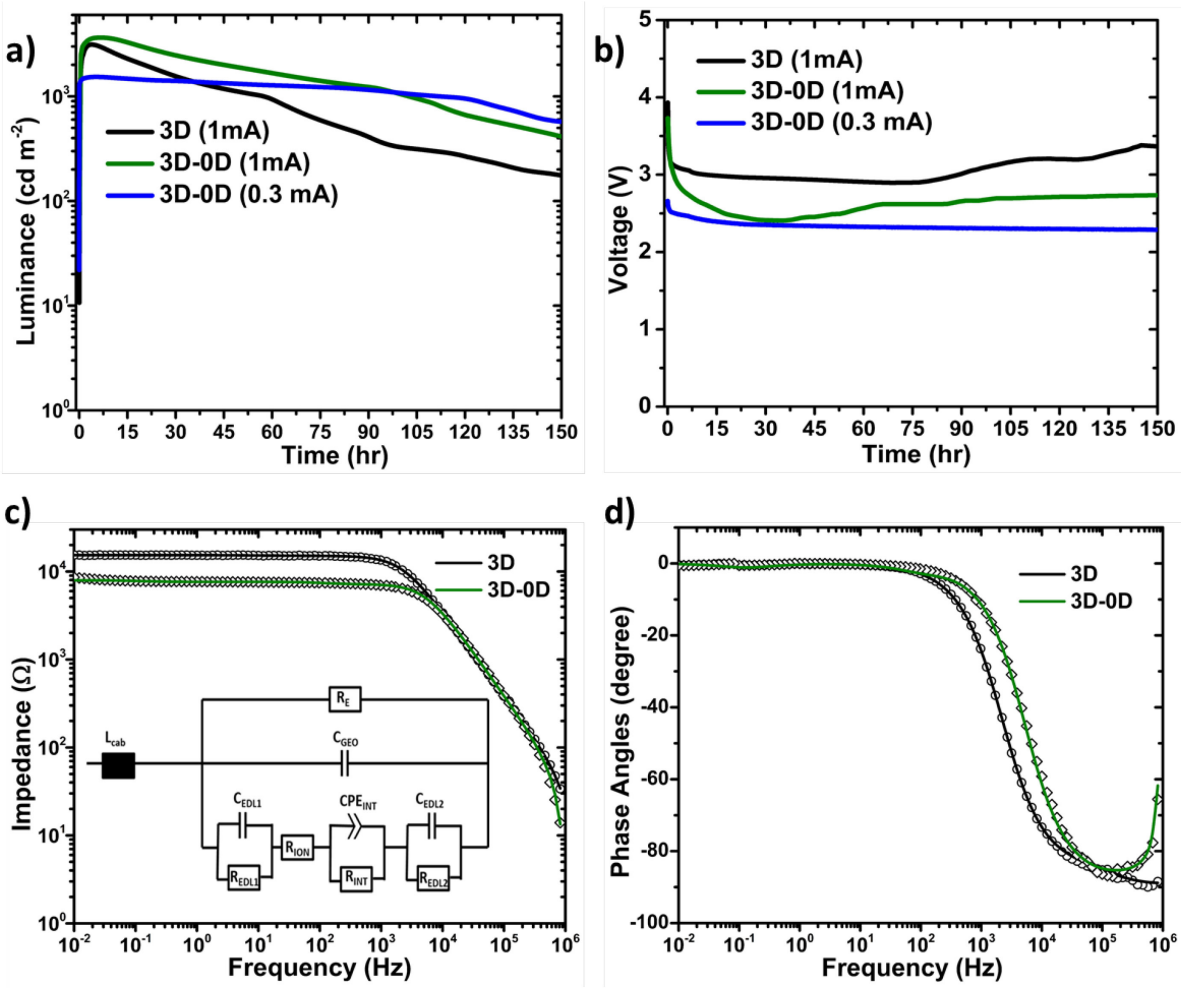

Figure 3. Constant current density and electrochemical impedance characteristics of 3D and 3D-0D (high PLQY) PeLECs. a) Luminance versus time for 3D and 3D-0D (high PLQY) PeLECs at 33.3 mA cm^{-2} and a 3D-0D (high PLQY) PeLEC at 10 mA cm^{-2} constant current density. b) Voltage versus time for 3D and 3D-0D (high PLQY) PeLECs at 33.3 mA cm^{-2} and a 3D-0D (high PLQY) PeLEC at 10 mA cm^{-2} constant current density. c) Complex impedance magnitude versus frequency for 3D and 3D-0D (high PLQY) PeLECs. Solid lines are equivalent circuit fits to the data. (Inset: equivalent circuit model.) d) Complex impedance phase angle versus frequency for 3D and 3D-0D (high PLQY) PeLECs. Solid lines are equivalent circuit fits to the data.

The mounting evidence of improved ionic redistribution and electronic conductivity from 0D emissive PNCs inclusion led us to investigate the phenomenon by electrochemical impedance spectroscopy and fitting with an equivalent circuit model. The complex impedance for 3D and 3D-0D PeLECs is plotted as the magnitude and phase angle versus frequency in Figure 3c and 3d, respectively. The equivalent circuit model used to fit the curve is shown as the inset in Figure 3c, a model that has previously fitted PeLEC operation.[17c] At low frequencies (<1 kHz), the 3D-0D PeLEC exhibits a lower impedance than the 3D counterpart (Figure 3c). The corner frequency increases from 2 kHz for the 3D PeLEC to 10 kHz for the 3D-0D PeLEC, a substantial improvement consistent with a greater ionic (capacitive) response. Similarly, the trend toward higher phase angles and more complex behavior is shifted to higher frequencies for the 3D-0D blend in Figure 3d.

The equivalent circuit model provides an excellent fit to the impedance curves (solid lines of Figure 3c and 3d), and the parameters extracted from this fitting according to previously discussed methods[17c, 22] are shown in **Table 1**. In short, this equivalent circuit accounts for an overall resistance, an overall geometric capacitance, double layer formation at each contact with a resistor and capacitor in parallel, and internal ionic effects. The conductivity of the 3D-0D device is 75% higher than the 3D-only PeLEC analog. The dielectric constant is reduced from 15.3 for the 3D PeLEC to 10.8 for the 3D-0D blend, consistent with the strongly-bound excitons of the 0D component[6,9c] and beneficial for enhanced luminance as Langevin recombination is inversely proportional to the dielectric constant.[22b] Concerning double layer formation, the capacitance increases with the 3D-0D blend, and the widths are decreased by ~40% relative to

the 3D device to 3.0 and 3.3 nm. The thinner widths are ideal for a narrower tunnel barrier for charge injection at each contact, and the symmetric barrier widths assist balanced injection for high recombination efficiency. The geometric capacitance decreases for the 3D-0D device, consistent with a greater participation of ions in double-layer formation. Hence, electrochemical impedance spectroscopy affirms the beneficial effects of 0D emissive PNC incorporation in the 3D matrix on electrical and ionic transport in PeLECs and additional factors that improve emission efficiency.

Table 1. Equivalent circuit and thin-film parameters extracted from electrochemical impedance spectroscopy analysis of 3D and 3D-0D (High PLQY) PeLECs.

Sample	Thickness [nm]	C_{GEO} [a)] [nF]	Dielectric Constant	C_{EDL1} [b)] [nF]	C_{EDL2} [c)] [nF]	W_{EDL1} [d)] [nm]	W_{EDL2} [e)] [nm]	Conductivity[f)] [μS m^{-1}]
3D	125	3.25	15.3	83	71	4.9	5.7	84.7
3D-0D	125	2.31	10.8	96	85	3.0	3.3	148

[a)]Geometric capacitance; [b)]Capacitance of EDL 1; [c)]Capacitance of EDL 2; [d)]Width of EDL 1; [e)]Width of EDL 2; [f)]Electrical conductivity

2.3 Structural characterization of 3D and 3D-0D perovskite thin films

It is important to physically characterize the thin film properties to ascertain if morphological effects also contribute to the superior performance of the 3D-0D emissive PNCs blends and verify the presence of each component. Notably, HRTEM and FFT analysis of 0D PNCs (high PLQY) confirm Cs_4PbBr_6 lattice planes [9d] and absence of any 3D impurity (Figure S3, Supporting Information). Alternative to these emissive PNCs, all the previous reports of 3D-0D composites or light-emitting devices involving a non-emissive 0D component involved changing the CsBr to $PbBr_2$ precursor ratio, where increasing the CsBr ratio led to more 0D phase formation, which in turn reduced the crystallite/grain size of the 3D part leading to increased confinement.[10b, 14b, 23] To compare our 3D-0D PNC blend with those from literature reports, we prepared composite films with an excess of CsBr (CsBr:$PbBr_2$ = 2:1 & 3:1) and

analyzed the structural details and device performance relative to the 3D and 3D-0D (High PLQY) PNC composite. As can be seen from the scanning electron microscopy (SEM) images provided in **Figure 4**a, the introduction of 0D (high PLQY) PNCs reduces the grain size significantly compared to the 3D film ($CsBr:PbBr_2$ = 1.5:1). In addition, both the 3D-0D film and the 3:1 precursor film showed a bimodal size distribution, while the 3D film was monomodal (Figure 4b). However, the films appeared smoothest and having the fewest pinholes for the 3D-0D film. This assertion can be further confirmed from the atomic force microcopy (AFM) images provided in Figure 4c. The incorporation of 0D PNCs reduces the surface roughness almost twofold, from 15 nm to 8.0 nm compared to 3D film (Figure 4c and 4d). Additionally, the 3D-0D (High PLQY) PNC film shows tighter packing and evidence of fewer pinholes. These features are all beneficial for suppressed leakage current leading to higher quantum efficiencies and greater device reliability. However, since the composites involving high PLQY, low PLQY, and non-emissive 0D PNCs show similar morphology (Figure S4 and S5, Supporting Information), and yet a significant difference in the performance of the corresponding PeLECs, the emission PLQY of the 0D PNCs indeed plays a crucial role along with the change in morphology. It is important to mention here that unlike literature reports where the thin film morphology is mostly dominated by larger 0D grains which encapsulate/act as a matrix for smaller 3D grains, in our case, only ~7 wt% addition of 0D PNCs compared to 3D implies that the grains we observe in the SEM images are still originated primarily from the 3D part.

To further confirm the ratios between 0D and 3D components, we analyzed the X-ray diffraction patterns (XRD) of the same samples, along with the films prepared by varying CsBr and $PbBr_2$ ratios. As shown in Figure 4e, the 3D film ($CsBr:PbBr_2$ = 1.5:1) showed major diffraction peaks at 15.3°, 21.5°, and 30.7°, in agreement with previous reports for an orthorhombic (Pnma) crystal structure.[24] (See Figure S6, Supporting Information for

additional XRD patterns). With an increase in the CsBr:$PbBr_2$ ratio, the XRD shows an appearance and consecutive increase of characteristic 0D Cs_4PbBr_6 peaks at 12.7° and 22.4° (marked red).[10b, 23] The most intense 0D peaks were observed for CsBr:$PbBr_2$ ratio of 3:1, indicating an increased amount of 0D component in the composite. However, for the 3D-0D PNC blend, the ratio of 0D peaks relative to 3D remains negligible, which agrees with the presence of a low weight percentage of 0D PNCs relative to 3D.

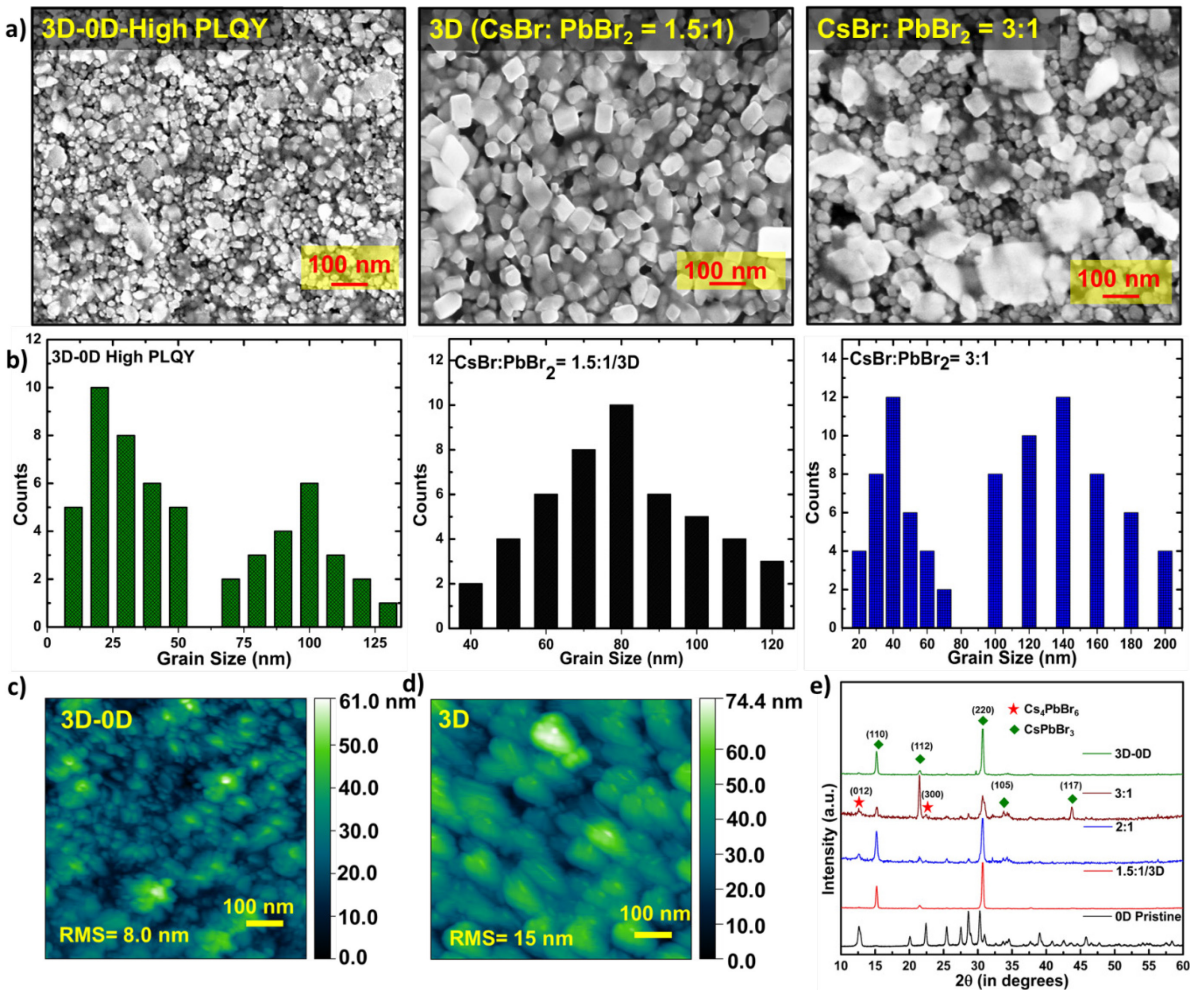

Figure 4. a) SEM of thin films of 3D-0D (high PLQY) perovskites, as well as the 3D-only (CsBr:$PbBr_2$ = 1.5:1) film and a film cast from a different precursor ratio (CsBr:$PbBr_2$ = 3:1) to spontaneously produce 0D phases in the 3D matrix. Additional SEM images are in Figure S4, Supporting Information. b) Size distribution analysis from SEM of various perovskite thin films. c) Atomic force microscopy of a thin film of 3D-0D (high PLQY) perovskites. d) Atomic force microscopy of a thin 3D perovskite film. e) XRD of thin films of emissive 0D PNCs (high PLQY) and different composite 3D-0D perovskite films, including those from various CsBr:$PbBr_2$ precursor ratios.

2.4 3D-0D PeLECs Fabricated Using Different Precursor Ratios

To clarify how incorporating highly emissive 0D PNCs in our case impacts device operation compared to non-emissive Cs_4PbBr_6 formed from a high CsBr:$PbBr_2$ ratio, we analyzed the performance of corresponding 3D-0D PeLECs. **Figure 5** compares the L-I-V PeLEC performance of the 3D only film (CsBr:$PbBr_2$ 1.5:1) with devices prepared from CsBr:$PbBr_2$ precursor formulations of 2:1 and 3:1 having a significant 0D phase as observed in XRD. These spontaneous 3D-0D films allow us to compare their performance to the 3D-0D devices from pre-synthesized 0D PNCs of low and high PLQY (Figure 2). From the current density vs. voltage curve provided in Figure 5a, it is obvious that an increase in the amount of CsBr does not suppress the leakage current or improve the charge injection as observed for incorporating 0D PNCs. In the luminance versus voltage graph of Figure 5b, the turn-on voltage is increased for 2:1 and 3:1 precursor films, and the peak luminance is lowered relative to the 1.5:1 3D-only phase. The EQE vs. voltage plot (Figure 5b, inset) shows that the EQE peak values fall from 2.7% for the 3D-only device to 2.5% for the 2:1 phase and 2.3% for the 3:1 phase. Thus, the spontaneous 0D phase formation from higher CsBr:$PbBr_2$ precursor formulations does not benefit device performance in our case, likely due to their non-luminescent nature. This lowered performance highlights the contrasting improved light-emitting performance of 3D-0D composite originating from our pre-synthesized PNCs compared to the typical approach of previous literature reports.

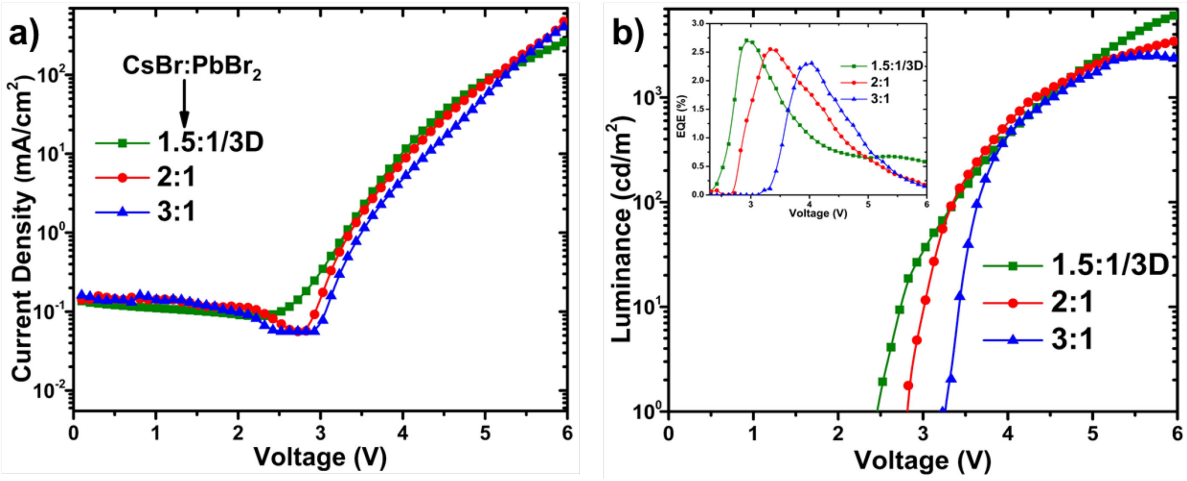

Figure 5. Luminance-current-voltage characteristics of PeLECs formed from different CsBr:$PbBr_2$ precursor ratios. a) Current density vs. voltage for PeLECs formed from different CsBr:$PbBr_2$ precursor ratios. b) Luminance vs. voltage for PeLECs formed from different CsBr:$PbBr_2$ precursor ratios. (Inset: EQE versus voltage for PeLECs formed from different CsBr:$PbBr_2$ precursor ratios.)

3. Conclusion

In summary, we demonstrated that incorporation of an optimized amount of highly emissive 0D Cs_4PbBr_6 PNCs into 3D $CsPbBr_3$ PeLECs using a novel solvent engineering method dramatically improves the maximum luminance (11200 cd m^{-2}), power (33.0 Lm W^{-1}), and quantum efficiency (8.3%), as well as the operational stability (129 h at 10 mA cm^{-2}) of the device. This operational stability is among the best for perovskite electroluminescent devices. It also improves the film morphology by reducing grain size, surface roughness, and the number of pinholes, resulting in suppressed leakage current. Contrary to all the previous reports of light-emitting devices involving 3D $CsPbBr_3$-0D Cs_4PbBr_6 materials where non-emissive 0D part acts mostly as a surface passivating matrix to provide quantum/dielectric confinement, the high intrinsic luminescence of the 0D PNCs plays a crucial role in significantly enhancing the luminance of our composites. This approach opens numerous avenues to explore 0D Cs_4PbBr_6 PNCs for high-performance electroluminescent devices.

4. Experimental Section/Methods

Materials: Cesium bromide (CsBr; 99.99%) and polyethylene oxide (PEO; M.W. > 5,000,000) were purchased from Alfa Aesar. Cesium carbonate (Cs_2CO_3, 99%), lead bromide ($PbBr_2$, >98%), oleic acid (OA, 90%), oleylamine (OLA, 90%), N,N-dimethylformamide (DMF, 99.8%), 1,2-dichlorobenzene (DCB, anhydrous, 99%), n-hexane (anhydrous, 99.98%), Lead (II) bromide ($PbBr_2$; 99.99% trace metal basis), Lithium hexafluorophosphate ($LiPF_6$; 99.99%) and dimethyl sulfoxide (DMSO; anhydrous > 99.9 %) were purchased from Sigma Aldrich. ITO-coated glass slides were purchased from Thin Film Devices, Inc. (Anaheim, CA). Aluminum (99.99%) was purchased from Kurt J. Lesker. LiF was purchased from Sigma Aldrich.

Synthesis of emissive Cs_4PbBr_6 PNCs: Emissive Cs_4PbBr_6 PNCs were synthesized using reverse microemulsion method.[9c] In a typical procedure, the $PbBr_2$ precursor and the Cs-oleate precursor were synthesized separately. First, a mixture of 2.25 g of Cs_2CO_3 and 21.5 mL of OA were stirred and degassed at 130 °C under vacuum for 1 hour to generate a yellowish stock of Cs-oleate precursor. Second, 0.2 mL Cs-oleate precursor, 10 mL n-hexane, 5 mL OA were loaded in a 50-mL three-neck flask, followed by mild degassing and nitrogen purging. Third, into the flask, a mixture of $PbBr_2$ (0.03 M, DMF, 1 mL), HBr (48 wt%, 15 μL), 0.1 mL OA, and 0.05 mL OLA was swiftly injected under vigorous stirring. A color change from pale-white to green was observed in 10 min, suggesting the formation of Cs_4PbBr_6 PNCs. The HBr amount was varied to achieve PNCs with different PLQY.[9d] The as-synthesized nanocrystals were collected via centrifugation at 8000 rpm for 3 min (one-centrifugation-only purification process), followed by dispersion in 2 mL of toluene for further characterization.

Synthesis of non-emissive Cs_4PbBr_6 PNCs: Non-emissive Cs_4PbBr_6 PNCs were synthesized following a literature reported procedure.[7b] In a typical synthesis, $PbBr_2$ (0.1 mmol) was dissolved in 5 mL ODE, 0.2 mL OA and 1.5 mL OLA in a 20 mL vial on a hotplate set at 150 °C. After the $PbBr_2$ was completely dissolved (around 100 ºC), the vial was allowed to cool. When the temperature reached 80 ºC, 0.75 mL of Cs-OA (0.4 g Cs_2CO_3 dissolved in 8 mL OA in a 20 ml vial on a hotplate set to 150 ºC) was swiftly injected. After about 30 seconds the mixture turned turbid white and the vial was quickly cooled down after 8 min to RT by immersion in a cold water bath. The PNCs were directly washed by centrifugation (at 4500 rpm for 10 minutes), followed by redispersion in 6 ml toluene for further characterizations.

Solution preparation: The $CsPbBr_3$ precursor solution was prepared by dissolving CsBr:$PbBr_2$ in various molar ratios (ranging from 1.5:1 to 3:1) in DMSO and kept overnight for dissolution. PEO (10mg/ml) was dissolved in DMSO. The $CsPbBr_3$ and PEO solutions were mixed in a 5:4 weight ratio. $LiPF_6$ salt (4mg/ml in DMSO) was added to this solution in a 0.5% weight ratio.

Device fabrication: The ITO/glass substrates (~20 Ω sq^{-1}) were cleaned in a sequence of non-ionic detergent wash, water bath sonication, and UV ozone treatment. Aqueous poly(3,4-ethylenedioxythiophene):polystyrene sulfonate (PEDOT:PSS) solutions (1.3−1.7%, Clevios AI 4083) were filtered through a 0.45 μm GHP filter and then spin-coated to obtain a ∼20 nm thick film on the ITO-coated glass substrates. These films were subsequently annealed at 100 °C for 10 minutes in a dry N_2-filled glovebox. The prepared active layer precursor solution was spin

cast onto the PEDOT:PSS layer at 1500rpm for 75 seconds, and after this time most of the DMSO is rinsed off from the 3D spin-coated films. Dispersed 0D PNCs in HFE (3M Novec 7500, 6-15 mg/ml) were introduced after 75th sec of spin coating and allowed to rest for 10 sec for proper mixing of 0D PNCs into 3D matrix followed by 30-sec spin coating at 2000 rpm. The spin-coated 3D-0D film was vacuum treated for 150 seconds to allow all the solvents to be evaporated and then thermally annealed at 150 °C for 35 sec to obtain a crystalline 3D-0D thin film. The active layer thicknesses were generally 125-130 nm. To deposit the top electrode, samples were transferred to a vacuum chamber, and 10 Å LiF and 800 Å Al were deposited using a shadow mask that defined 12 devices per substrate, each with a 3 mm^2 device area.

Electroluminescence measurements: The current-voltage electrical characteristics were obtained with a 760D electrochemical analyzer from CH Instruments (Austin, TX), with radiant exitance measurements acquired with a calibrated Labsphere integrating sphere equipped with a thermoelectric-cooled silicon photodetector and Keithley 6485 picoammeter. Each cyclic LIV sweep was performed at 0.1V/sec with 5 seconds of interval between each scan. Electroluminescence spectra were measured with an Ocean Optics Jazz fiber spectrometer. Lifetime measurements were obtained with a custom multiplexer testing station capable of measuring 16 light emitting devices simultaneously. In brief, this instrument supplied constant current and measured voltage with custom circuitry and simultaneously captured radiant flux with a calibrated Hamamatsu photodiode (S2387-1010R) for each device.

Scanning Electron Microscopy (SEM): Secondary electron SEM images were taken with a Zeiss Supra-40 SEM using an in-lens detector at an accelerating voltage of 10kV.

Atomic Force Microscopy (AFM): The AFM images were performed using a Veeco Model 3100 Dimension V to scrutinize the morphology of thin films. The thin films were scanned for 5µm × 5µm area at 0.8Hz rate using an OTESPA-R3 AFM tip from Bruker. Tapping mode AFM was used for this characterization.

X-Ray Diffraction (XRD): XRD measurements were collected using a Rigaku SmartLab X-ray Cu target (K_α=1.5418 Å) and a HyPix 3000 detector. The 2-theta/omega scan was consistently performed in the 2-theta range of 10° to 55° with a 0.01° step and a ~1°/min scan speed.

High-Resolution Transmission Electron Microscopy (HRTEM): Low-dose HRTEM images were acquired with a Gatan K2 Summit direct-detection electron-counting (DDEC) camera on a Cs-corrected Titan cubed G2 60-300 electron microscope at 300 kV. A stack of successive short-exposure frames (0.05 s frame^{-1}, and 120 frames) was recorded on each particle at extremely low doses (~30-40 e A^{-2}). Drift between frames was corrected based on literature methods.[25]

Statistical Analysis: Statistical analysis of PeLEC maximum luminance and EQE was performed and is plotted in Figure S2, Supporting Information. No pre-processing of data was performed. Data is presented as the mean ± standard deviation for n = 12 devices. A two-tailed t test was performed with Excel, and p values were reported.

Supporting Information

Supporting Information is available from the Wiley Online Library or from the author.

Conflicts of Interest

The authors declare no conflicts of interest.

Data Availability

The data that support the findings of this study are available from the corresponding author upon reasonable request.

Acknowledgements

J.D.S. acknowledges support from the National Science Foundation (ECCS 1906505). R.B., Y.Z., and A.V.M. were supported by the U.S. Department of Energy, Office of Basic Energy Sciences, Division of Materials Sciences and Engineering (DE-SC0010697). W.X. and J.W.P.H. acknowledge the support of Texas Instruments Distinguished Chair of Nanoelectronics. The authors would also like to thank Kepeng Song of Shandong University for assistance with the HRTEM.

References

[1] a) M. M. Lee, J. Teuscher, T. Miyasaka, T. N. Murakami, H. J. Snaith, *Science* **2012**, 338, 643; b) M. Liu, M. B. Johnston, H. J. Snaith, *Nature* **2013**, 501, 395; c) J. H. Heo, S. H. Im, J. H. Noh, T. N. Mandal, C.-S. Lim, J. A. Chang, Y. H. Lee, H.-j. Kim, A. Sarkar, M. K. Nazeeruddin, M. Grätzel, S. I. Seok, *Nat. Photonics* **2013**, 7, 486; d) N.

J. Jeon, J. H. Noh, Y. C. Kim, W. S. Yang, S. Ryu, S. I. Seok, *Nat. Mater.* **2014**, 13, 897; e) F. Deschler, M. Price, S. Pathak, L. E. Klintberg, D.-D. Jarausch, R. Higler, S. Hüttner, T. Leijtens, S. D. Stranks, H. J. Snaith, M. Atatüre, R. T. Phillips, R. H. Friend, *J. Phys. Chem. Lett.* **2014**, 5, 1421; f) Z.-K. Tan, R. S. Moghaddam, M. L. Lai, P. Docampo, R. Higler, F. Deschler, M. Price, A. Sadhanala, L. M. Pazos, D. Credgington, F. Hanusch, T. Bein, H. J. Snaith, R. H. Friend, *Nat. Nanotechnol.* **2014**, 9, 687; g) S. D. Stranks, H. J. Snaith, *Nat. Nanotechnol.* **2015**, 10, 391; h) F. Meinardi, Q. A. Akkerman, F. Bruni, S. Park, M. Mauri, Z. Dang, L. Manna, S. Brovelli, *ACS Energy Lett.* **2017**, 2, 2368; i) I. Dursun, C. Shen, M. R. Parida, J. Pan, S. P. Sarmah, D. Priante, N. Alyami, J. Liu, M. I. Saidaminov, M. S. Alias, A. L. Abdelhady, T. K. Ng, O. F. Mohammed, B. S. Ooi, O. M. Bakr, *ACS Photonics* **2016**, 3, 1150; j) D. N. Congreve, M. C. Weidman, M. Seitz, W. Paritmongkol, N. S. Dahod, W. A. Tisdale, *ACS Photonics* **2017**, 4, 476; k) H. Wang, D. H. Kim, *Chem. Soc. Rev.* **2017**, 46, 5204.

[2] a) L. Protesescu, S. Yakunin, M. I. Bodnarchuk, F. Krieg, R. Caputo, C. H. Hendon, R. X. Yang, A. Walsh, M. V. Kovalenko, *Nano Lett.* **2015**, 15, 3692; b) N. Yantara, S. Bhaumik, F. Yan, D. Sabba, H. A. Dewi, N. Mathews, P. P. Boix, H. V. Demir, S. Mhaisalkar, *J. Phys. Chem. Lett.* **2015**, 6, 4360; c) X. Li, Y. Wu, S. Zhang, B. Cai, Y. Gu, J. Song, H. Zeng, *Adv. Funct. Mater.* **2016**, 26, 2435; d) Y. Tong, E. Bladt, M. F. Aygüler, A. Manzi, K. Z. Milowska, V. A. Hintermayr, P. Docampo, S. Bals, A. S. Urban, L. Polavarapu, J. Feldmann, *Angew. Chem.-Int. Ed.* **2016**, 55, 13887; e) J. Song, J. Li, X. Li, L. Xu, Y. Dong, H. Zeng, *Adv. Mater.* **2015**, 27, 7162; f) A. Swarnkar, R. Chulliyil, V. K. Ravi, M. Irfanullah, A. Chowdhury, A. Nag, *Angew. Chem.-Int. Ed.* **2015**, 54, 15424; g) G. Li, F. W. R. Rivarola, N. J. L. K. Davis, S. Bai, T. C. Jellicoe, F. de la Peña, S. Hou, C. Ducati, F. Gao, R. H. Friend, N. C. Greenham, Z.-K. Tan, *Adv. Mater.* **2016**, 28, 3528; h) X. Zhang, C. Sun, Y. Zhang, H. Wu, C. Ji, Y. Chuai, P. Wang, S. Wen, C. Zhang, W. W. Yu, *J. Phys. Chem. Lett.* **2016**, 7, 4602; i) J. Si, Y. Liu, Z. He, H. Du, K. Du, D. Chen, J. Li, M. Xu, H. Tian, H. He, D. Di, C. Lin, Y. Cheng, J. Wang, Y. Jin, *ACS Nano* **2017**, 11, 11100; j) E. Yassitepe, Z. Yang, O. Voznyy, Y. Kim, G. Walters, J. A. Castañeda, P. Kanjanaboos, M. Yuan, X. Gong, F. Fan, J. Pan, S. Hoogland, R. Comin, O. M. Bakr, L. A. Padilha, A. F. Nogueira, E. H. Sargent, *Adv. Funct. Mater.* **2016**, 26, 8757; k) Y. Shen, L.-P. Cheng, Y.-Q. Li, W. Li, J.-D. Chen, S.-T. Lee, J.-X. Tang, *Adv. Mater.* **2019**, 31, 1901517; l) Y.-K. Wang, F. Yuan, Y. Dong, J.-Y. Li, A. Johnston, B. Chen, M. I. Saidaminov, C. Zhou, X. Zheng, Y. Hou, K. Bertens, H. Ebe, D. Ma, Z. Deng, S. Yuan, R. Chen, L. K. Sagar, J. Liu, J. Fan, P. Li, X. Li, Y. Gao, M.-K. Fung, Z.-H. Lu, O. M. Bakr, L.-S. Liao, E. H. Sargent, *Angew. Chem.-Int. Ed.* **2021**, 60, 16164.

[3] a) K. B. Lin, J. Xing, L. N. Quan, F. P. G. de Arquer, X. W. Gong, J. X. Lu, L. Q. Xie, W. J. Zhao, D. Zhang, C. Z. Yan, W. Q. Li, X. Y. Liu, Y. Lu, J. Kirman, E. H. Sargent, Q. H. Xiong, Z. H. Wei, *Nature* **2018**, 562, 245; b) L. N. Quan, B. P. Rand, R. H. Friend, S. G. Mhaisalkar, T. W. Lee, E. H. Sargent, *Chem. Rev.* **2019**, 119, 7444; c) Y. Cao, N. Wang, H. Tian, J. Guo, Y. Wei, H. Chen, Y. Miao, W. Zou, K. Pan, Y. He, H. Cao, Y. Ke, M. Xu, Y. Wang, M. Yang, K. Du, Z. Fu, D. Kong, D. Dai, Y. Jin, G. Li, H. Li, Q. Peng, J. Wang, W. Huang, *Nature* **2018**, 562, 249; d) B. Zhao, Y. Lian, L. Cui, G. Divitini, G. Kusch, E. Ruggeri, F. Auras, W. Li, D. Yang, B. Zhu, R. A. Oliver, J. L. MacManus-Driscoll, S. D. Stranks, D. Di, R. H. Friend, *Nat. Electron.* **2020**, 3, 704; e) H. C. Cho, S. H. Jeong, M. H. Park, Y. H. Kim, C. Wolf, C. L. Lee, J. H. Heo, A. Sadhanala, N. Myoung, S. Yoo, S. H. Im, R. H. Friend, T. W. Lee, *Science* **2015**, 350, 1222; f) Z. Fang, W. Chen, Y. Shi, J. Zhao, S. Chu, J. Zhang, Z. Xiao, *Adv. Funct. Mater.* **2020**, 30, 1909754; g) Y.-H. Kim, S. Kim, A. Kakekhani, J. Park, J. Park, Y.-H. Lee, H. Xu, S. Nagane, R. B. Wexler, D.-H. Kim, S. H. Jo, L. Martínez-Sarti, P. Tan, A. Sadhanala, G.-S. Park, Y.-W. Kim, B. Hu, H. J. Bolink, S.

Yoo, R. H. Friend, A. M. Rappe, T.-W. Lee, *Nat. Photonics* **2021**, 15, 148; h) T. Chiba, Y. Hayashi, H. Ebe, K. Hoshi, J. Sato, S. Sato, Y.-J. Pu, S. Ohisa, J. Kido, *Nat. Photonics* **2018**, 12, 681; i) X. Zhao, Z.-K. Tan, *Nat. Photonics* **2020**, 14, 215.

[4] a) Y. Dong, Y.-K. Wang, F. Yuan, A. Johnston, Y. Liu, D. Ma, M.-J. Choi, B. Chen, M. Chekini, S.-W. Baek, L. K. Sagar, J. Fan, Y. Hou, M. Wu, S. Lee, B. Sun, S. Hoogland, R. Quintero-Bermudez, H. Ebe, P. Todorovic, F. Dinic, P. Li, H. T. Kung, M. I. Saidaminov, E. Kumacheva, E. Spiecker, L.-S. Liao, O. Voznyy, Z.-H. Lu, E. H. Sargent, *Nat. Nanotechnol.* **2020**, 15, 668; b) C. Wu, Y. Zou, T. Wu, M. Ban, V. Pecunia, Y. Han, Q. Liu, T. Song, S. Duhm, B. Sun, *Adv. Funct. Mater.* **2017**, 27, 1700338; c) D. Yang, X. Li, H. Zeng, *Adv. Mater. Interfaces* **2018**, 5, 1701662; d) R. Grisorio, M. E. Di Clemente, E. Fanizza, I. Allegretta, D. Altamura, M. Striccoli, R. Terzano, C. Giannini, M. Irimia-Vladu, G. P. Suranna, *Nanoscale* **2019**, 11, 986.

[5] a) K. Lin, J. Xing, L. N. Quan, F. P. G. de Arquer, X. Gong, J. Lu, L. Xie, W. Zhao, D. Zhang, C. Yan, W. Li, X. Liu, Y. Lu, J. Kirman, E. H. Sargent, Q. Xiong, Z. Wei, *Nature* **2018**, 562, 245; b) J. Song, J. Li, L. Xu, J. Li, F. Zhang, B. Han, Q. Shan, H. Zeng, *Adv. Mater.* **2018**, 30, 1800764; c) P. Liu, W. Chen, W. Wang, B. Xu, D. Wu, J. Hao, W. Cao, F. Fang, Y. Li, Y. Zeng, R. Pan, S. Chen, W. Cao, X. W. Sun, K. Wang, *Chem. Mat.* **2017**, 29, 5168; d) W. Cai, Z. Chen, D. Chen, S. Su, Q. Xu, H.-L. Yip, Y. Cao, *RSC Adv.* **2019**, 9, 27684; e) Y.-K. Wang, D. Ma, F. Yuan, K. Singh, J. M. Pina, A. Johnston, Y. Dong, C. Zhou, B. Chen, B. Sun, H. Ebe, J. Fan, M.-J. Sun, Y. Gao, Z.-H. Lu, O. Voznyy, L.-S. Liao, E. H. Sargent, *Nat. Commun.* **2020**, 11, 3674; f) S. Zou, Y. Liu, J. Li, C. Liu, R. Feng, F. Jiang, Y. Li, J. Song, H. Zeng, M. Hong, X. Chen, *J. Am. Chem. Soc.* **2017**, 139, 11443; g) X. Zhou, Y. Zhao, W. Huang, Y. Wu, Z. Wu, G. He, *Org. Electron.* **2021**, 96, 106253; h) J. Song, T. Fang, J. Li, L. Xu, F. Zhang, B. Han, Q. Shan, H. Zeng, *Adv. Mater.* **2018**, 30, 1805409; i) H. Wang, X. Zhang, Q. Wu, F. Cao, D. Yang, Y. Shang, Z. Ning, W. Zhang, W. Zheng, Y. Yan, S. V. Kershaw, L. Zhang, A. L. Rogach, X. Yang, *Nat. Commun.* **2019**, 10, 665; j) J. Li, L. Xu, T. Wang, J. Song, J. Chen, J. Xue, Y. Dong, B. Cai, Q. Shan, B. Han, H. Zeng, *Adv. Mater.* **2017**, 29, 1603885; k) C. Sun, Y. Zhang, C. Ruan, C. Yin, X. Wang, Y. Wang, W. W. Yu, *Adv. Mater.* **2016**, 28, 10088.

[6] a) M. I. Saidaminov, O. F. Mohammed, O. M. Bakr, *ACS Energy Lett.* **2017**, 2, 889; b) J. Almutlaq, J. Yin, O. F. Mohammed, O. M. Bakr, *J. Phys. Chem. Lett.* **2018**, 9, 4131; c) P. Arunkumar, H. B. Cho, K. H. Gil, S. Unithrattil, Y. H. Kim, W. Bin Im, *Nat. Commun.* **2018**, 9, 4691; d) Q. A. Akkerman, A. L. Abdelhady, L. Manna, *J. Phys. Chem. Lett.* **2018**, 9, 2326.

[7] a) L. Wu, H. Hu, Y. Xu, S. Jiang, M. Chen, Q. Zhong, D. Yang, Q. Liu, Y. Zhao, B. Sun, Q. Zhang, Y. Yin, *Nano Lett.* **2017**, 17, 5799; b) F. Palazon, C. Urso, L. De Trizio, Q. Akkerman, S. Marras, F. Locardi, I. Nelli, M. Ferretti, M. Prato, L. Manna, *ACS Energy Lett.* **2017**, 2, 2445; c) M. Shin, S.-W. Nam, A. Sadhanala, R. Shivanna, M. Anaya, A. Jiménez-Solano, H. Yoon, S. Jeon, S. D. Stranks, R. L. Z. Hoye, B. Shin, *ACS Applied Energy Materials* **2020**, 3, 192; d) Q. A. Akkerman, S. Park, E. Radicchi, F. Nunzi, E. Mosconi, F. De Angelis, R. Brescia, P. Rastogi, M. Prato, L. Manna, *Nano Lett.* **2017**, 17, 1924; e) D. Han, H. Shi, W. Ming, C. Zhou, B. Ma, B. Saparov, Y.-Z. Ma, S. Chen, M.-H. Du, *J. Mater. Chem. C* **2018**, 6, 6398; f) Z. Qin, S. Dai, V. G. Hadjiev, C. Wang, L. Xie, Y. Ni, C. Wu, G. Yang, S. Chen, L. Deng, Q. Yu, G. Feng, Z. M. Wang, J. Bao, *Chem. Mat.* **2019**, 31, 9098; g) N. Riesen, M. Lockrey, K. Badek, H. Riesen, *Nanoscale* **2019**, 11, 3925.

[8] a) S. Seth, A. Samanta, *J. Phys. Chem. Lett.* **2017**, 8, 4461; b) M. De Bastiani, I. Dursun, Y. Zhang, B. A. Alshankiti, X.-H. Miao, J. Yin, E. Yengel, E. Alarousu, B. Turedi, J. M. Almutlaq, M. I. Saidaminov, S. Mitra, I. Gereige, A. AlSaggaf, Y. Zhu, Y. Han, I. S. Roqan, J.-L. Bredas, O. F. Mohammed, O. M. Bakr, *Chem. Mat.* **2017**,

29, 7108; c) S. Seth, A. Samanta, *J. Phys. Chem. Lett.* **2018**, 9, 176; d) J. Yin, P. Maity, M. De Bastiani, I. Dursun, O. M. Bakr, J.-L. Brédas, O. F. Mohammed, *Sci. Adv.* **2017**, 3, e1701793; e) P. Pal, S. Saha, A. Banik, A. Sarkar, K. Biswas, *Chemistry – A European Journal* **2018**, 24, 1811; f) H. Zhang, Q. Liao, Y. Wu, J. Chen, Q. Gao, H. Fu, *Phys. Chem. Chem. Phys.* **2017**, 19, 29092; g) Y.-K. Jung, J. Calbo, J.-S. Park, L. D. Whalley, S. Kim, A. Walsh, *Journal of Materials Chemistry A* **2019**, 7, 20254; h) M. Hu, C. Ge, J. Yu, J. Feng, *J. Phys. Chem. C* **2017**, 121, 27053.

[9] a) M. I. Saidaminov, J. Almutlaq, S. Sarmah, I. Dursun, A. A. Zhumekenov, R. Begum, J. Pan, N. Cho, O. F. Mohammed, O. M. Bakr, *ACS Energy Lett.* **2016**, 1, 840; b) D. Chen, Z. Wan, X. Chen, Y. Yuan, J. Zhong, *J. Mater. Chem. C* **2016**, 4, 10646; c) Y. Zhang, M. I. Saidaminov, I. Dursun, H. Yang, B. Murali, E. Alarousu, E. Yengel, B. A. Alshankiti, O. M. Bakr, O. F. Mohammed, *J. Phys. Chem. Lett.* **2017**, 8, 961; d) J. Yin, H. Yang, K. Song, A. M. El-Zohry, Y. Han, O. M. Bakr, J.-L. Brédas, O. F. Mohammed, *J. Phys. Chem. Lett.* **2018**, 9, 5490; e) J. Zhang, A. Wang, L. Kong, L. Zhang, Z. Deng, *Journal of Alloys and Compounds* **2019**, 797, 1151; f) Y. Zhang, L. Sinatra, E. Alarousu, J. Yin, A. M. El-Zohry, O. M. Bakr, O. F. Mohammed, *J. Phys. Chem. C* **2018**, 122, 6493; g) Y. Zhang, T. Guo, H. Yang, R. Bose, L. Liu, J. Yin, Y. Han, O. M. Bakr, O. F. Mohammed, A. V. Malko, *Nat. Commun.* **2019**, 10, 2930.

[10] a) L. N. Quan, R. Quintero-Bermudez, O. Voznyy, G. Walters, A. Jain, J. Z. Fan, X. Zheng, Z. Yang, E. H. Sargent, *Adv. Mater.* **2017**, 29, 1605945; b) Z. Bao, H.-D. Chiu, W. Wang, Q. Su, T. Yamada, Y.-C. Chang, S. Chen, Y. Kanemitsu, R.-J. Chung, R.-S. Liu, *J. Phys. Chem. Lett.* **2020**, 11, 10196; c) Z. Bao, Y.-J. Tseng, W. You, W. Zheng, X. Chen, S. Mahlik, A. Lazarowska, T. Lesniewski, M. Grinberg, C. Ma, W. Sun, W. Zhou, R.-S. Liu, J. P. Attfield, *J. Phys. Chem. Lett.* **2020**, 11, 7637; d) M. He, C. Wang, J. Li, J. Wu, S. Zhang, H.-C. Kuo, L. Shao, S. Zhao, J. Zhang, F. Kang, G. Wei, *Nanoscale* **2019**, 11, 22899; e) W. Wang, D. Wang, F. Fang, S. Wang, G. Xu, T. Zhang, *Crystal Growth & Design* **2018**, 18, 6133; f) L. Xu, J. Li, T. Fang, Y. Zhao, S. Yuan, Y. Dong, J. Song, *Nanoscale Adv.* **2019**, 1, 980.

[11] a) Y. Ling, L. Tan, X. Wang, Y. Zhou, Y. Xin, B. Ma, K. Hanson, H. Gao, *J. Phys. Chem. Lett.* **2017**, 8, 3266; b) G. Jin, D. Zhang, P. Pang, Z. Ye, T. Liu, G. Xing, J. Chen, D. Ma, *J. Mater. Chem. C* **2021**, 9, 916; c) X. Chen, F. Zhang, Y. Ge, L. Shi, S. Huang, J. Tang, Z. Lv, L. Zhang, B. Zou, H. Zhong, *Adv. Funct. Mater.* **2018**, 28, 1706567.

[12] a) C.-Y. Huang, S.-H. Huang, C.-L. Wu, Z.-H. Wang, C.-C. Yang, *ACS Appl. Nano Mater.* **2020**, 3, 11760; b) Z. Wang, Y. Zhang, X. Liu, Y. Yu, F. Xu, J. Ding, X. Liang, K. Yang, W. Xiang, *Advanced Materials Technologies* **2021**, n/a, 2100654; c) X. Li, Z. Wen, S. Ding, F. Fang, B. Xu, J. Sun, C. Liu, K. Wang, X. W. Sun, *Adv. Opt. Mater.* **2020**, 8, 2000232; d) C. Jia, H. Li, X. Meng, H. Li, *Chem. Commun.* **2018**, 54, 6300.

[13] J. Xu, W. Huang, P. Li, D. R. Onken, C. Dun, Y. Guo, K. B. Ucer, C. Lu, H. Wang, S. M. Geyer, R. T. Williams, D. L. Carroll, *Adv. Mater.* **2017**, 29, 1703703.

[14] a) T. Xuan, S. Lou, J. Huang, L. Cao, X. Yang, H. Li, J. Wang, *Nanoscale* **2018**, 10, 9840; b) F. Cao, D. Yu, X. Xu, Z. Han, H. Zeng, *J. Phys. Chem. C* **2021**, 125, 3; c) G. Hu, W. Qin, M. Liu, X. Ren, X. Wu, L. Yang, S. Yin, *J. Mater. Chem. C* **2019**, 7, 4733.

[15] a) H. Lian, Y. Li, K. Sharafudeen, W. Zhao, G. R. Krishnan, S. Zhang, J. Qiu, K. Huang, G. Han, *Adv. Mater.* **2020**, 32, 2002495; b) S. Huang, S. Yang, Q. Wang, R. Wu, Q. Han, W. Wu, *RSC Adv.* **2019**, 9, 42430; c) Y. Wang, D. Yu, Z. Wang, X. Li, X. Chen, V. Nalla, H. Zeng, H. Sun, *Small* **2017**, 13, 1701587; d) F. Cao, D. Yu, W. Ma, X. Xu, B. Cai, Y. M. Yang, S. Liu, L. He, Y. Ke, S. Lan, K.-L. Choy, H. Zeng,

ACS Nano **2020**, 14, 5183; e) Z. Bao, J.-W. Luo, Y.-S. Wang, T.-C. Hu, S.-Y. Tsai, Y.-T. Tsai, H.-C. Wang, F.-H. Chen, Y.-C. Lee, T.-L. Tsai, R.-J. Chung, R.-S. Liu, *Chemical Engineering Journal* **2021**, 426, 130849; f) X. Lian, X. Wang, Y. Ling, E. Lochner, L. Tan, Y. Zhou, B. Ma, K. Hanson, H. Gao, *Adv. Funct. Mater.* **2019**, 29, 1807345; g) Q. Wang, W. Wu, R. Wu, S. Yang, Y. Wang, J. Wang, Z. Chai, Q. Han, *Journal of Colloid and Interface Science* **2019**, 554, 133.

[16] a) Z. Bao, H.-C. Wang, Z.-F. Jiang, R.-J. Chung, R.-S. Liu, *Inorg. Chem.* **2018**, 57, 13071; b) H. Zhao, R. Sun, Z. Wang, K. Fu, X. Hu, Y. Zhang, *Adv. Funct. Mater.* **2019**, 29, 1902262; c) X. Sun, Z. Gao, Y. Liu, Z. Wang, X. Wang, W. Zhang, B. Xu, X. Meng, *ACS Photonics* **2019**, 6, 3290; d) Y. Liu, X. Sun, Z. Gao, Y. Hou, K. Wang, W. Zhang, Z. Wang, X. Wang, B. Xu, X. Meng, *J. Phys. Chem. C* **2020**, 124, 25499; e) Y. Li, W. Shao, L. Chen, J. Wang, J. Nie, H. Zhang, S. Zhang, R. Gao, X. Ouyang, X. Ouyang, Q. Xu, *NPG Asia Materials* **2021**, 13, 40; f) J. Yang, Z. Liu, F. Zeng, M. Pi, T. Shi, Y. Bian, X. Tang, J. Du, W. Liu, Y. Leng, *Solar RRL* **2019**, 3, 1900127.

[17] a) P. Andricevic, X. Mettan, M. Kollar, B. Nafradi, A. Sienkiewicz, T. Garma, L. Rossi, L. Forro, E. Horvath, *ACS Photonics* **2019**, 6, 967; b) M. Alahbakhshi, A. Mishra, R. Haroldson, A. Ishteev, J. Moon, Q. Gu, J. D. Slinker, A. A. Zakhidov, *ACS Energy Lett.* **2019**, 4, 2922; c) A. Mishra, M. Alahbakhshi, R. Haroldson, L. D. Bastatas, Q. Gu, A. A. Zakhidov, J. D. Slinker, *Adv. Opt. Mater.* **2020**, 8, 2000226; d) A. Mishra, S. DiLuzio, M. Alahbakhshi, A. C. Adams, M. H. Bowler, J. Moon, Q. Gu, A. A. Zakhidov, S. Bernhard, J. D. Slinker, *Chem. Mat.* **2021**, 33, 1201; e) A. Mishra, M. Alahbakhshi, R. Haroldson, Q. Gu, A. A. Zakhidov, J. D. Slinker, *Adv. Funct. Mater.* **2021**, 31, 2102006; f) A. Mishra, M. Alahbakhshi, Q. Gu, A. A. Zakhidov, J. D. Slinker, *ACS Mater. Lett.* **2021**, 3, 1357; g) M. F. Ayguler, M. D. Weber, B. M. D. Puscher, D. D. Medina, P. Docampo, R. D. Costa, *J. Phys. Chem. C* **2015**, 119, 12047; h) H. M. Zhang, H. Lin, C. J. Liang, H. Liu, J. J. Liang, Y. Zhao, W. G. Zhang, M. J. Sun, W. K. Xiao, H. Li, S. Polizzi, D. Li, F. J. Zhang, Z. Q. He, W. C. H. Choy, *Adv. Funct. Mater.* **2015**, 25, 7226.

[18] a) Q. B. Pei, G. Yu, C. Zhang, Y. Yang, A. J. Heeger, *Science* **1995**, 269, 1086; b) J. C. deMello, *Physical Review B* **2002**, 66, 235210; c) J. D. Slinker, J. A. DeFranco, M. J. Jaquith, W. R. Silveira, Y. W. Zhong, J. M. Moran-Mirabal, H. G. Craighead, H. D. Abruna, J. A. Marohn, G. G. Malliaras, *Nat. Mater.* **2007**, 6, 894; d) R. D. Costa, E. Orti, H. J. Bolink, F. Monti, G. Accorsi, N. Armaroli, *Angew. Chem.-Int. Edit.* **2012**, 51, 8178; e) M. H. Bowler, A. Mishra, A. C. Adams, C. L.-D. Blangy, J. D. Slinker, *Adv. Funct. Mater.* **2020**, 30, 1906715; f) S. Hu, J. Gao, *Adv. Funct. Mater.* **2020**, 30, 1907003; g) K. Youssef, Y. Li, S. O'Keeffe, L. Li, Q. Pei, *Adv. Funct. Mater.* **2020**, 30, 1909102; h) E. Nannen, J. Frohleiks, S. Gellner, *Adv. Funct. Mater.* **2020**, 30, 1907349.

[19] a) A. A. Zakhidov, J.-K. Lee, H. H. Fong, J. A. DeFranco, M. Chatzichristidi, P. G. Taylor, C. K. Ober, G. G. Malliaras, *Adv. Mater.* **2008**, 20, 3481; b) M. Hasan, S. Venkatesan, D. Lyashenko, J. D. Slinker, A. Zakhidov, *Anal. Chem.* **2017**, 89, 9649.

[20] a) A. B. Tamayo, S. Garon, T. Sajoto, P. I. Djurovich, I. M. Tsyba, R. Bau, M. E. Thompson, *Inorg. Chem.* **2005**, 44, 8723; b) H.-C. Su, C.-C. Wu, F.-C. Fang, K.-T. Wong, *Appl. Phys. Lett.* **2006**, 89, 261118.

[21] a) H. Tsai, S. Shrestha, R. A. Vilá, W. Huang, C. Liu, C.-H. Hou, H.-H. Huang, X. Wen, M. Li, G. Wiederrecht, Y. Cui, M. Cotlet, X. Zhang, X. Ma, W. Nie, *Nat. Photonics* **2021**, 15, 843; b) T. Wu, J. Li, Y. Zou, H. Xu, K. Wen, S. Wan, S. Bai, T. Song, J. A. McLeod, S. Duhm, F. Gao, B. Sun, *Angew. Chem.-Int. Ed.* **2020**, 59, 4099.

[22] a) B. M. D. Puscher, M. F. Ayguler, P. Docampo, R. D. Costa, *Adv. Energy Mater.* **2017**, 7, 1602283; b) L. D. Bastatas, M. D. Moore, J. D. Slinker, *ChemPlusChem* **2018**, 83, 266.

[23] Y. Liu, S. Tang, J. Fan, E. Gracia-Espino, J. Yang, X. Liu, S. Kera, M. Fahlman, C. Larsen, T. Wågberg, L. Edman, J. Wang, *ACS Appl. Nano Mater.* **2021**, 4, 1162.

[24] a) T. G. Liashenko, E. D. Cherotchenko, A. P. Pushkarev, V. Pakštas, A. Naujokaitis, S. A. Khubezhov, R. G. Polozkov, K. B. Agapev, A. A. Zakhidov, I. A. Shelykh, S. V. Makarov, *Phys. Chem. Chem. Phys.* **2019**, 21, 18930; b) M. Zhang, Z. Zheng, Q. Fu, Z. Chen, J. He, S. Zhang, L. Yan, Y. Hu, W. Luo, *CrystEngComm* **2017**, 19, 6797; c) T. G. Liashenko, A. P. Pushkarev, A. Naujokaitis, V. Pakštas, M. Franckevičius, A. A. Zakhidov, S. V. Makarov, *Nanomaterials* **2020**, 10, 1937.

[25] D. Zhang, Y. Zhu, L. Liu, X. Ying, C.-E. Hsiung, R. Sougrat, K. Li, Y. Han, *Science* **2018**, 359, 675.

Aditya Mishra, Riya Bose, Yangzi Zheng, Weijie Xu, Reema McMullen, Julia W. P. Hsu, Anton V. Malko, and Jason D. Slinker*

Stable and Bright Electroluminescent Devices Utilizing Emissive 0D Perovskite Nanocrystals Incorporated in a 3D $CsPbBr_3$ Matrix

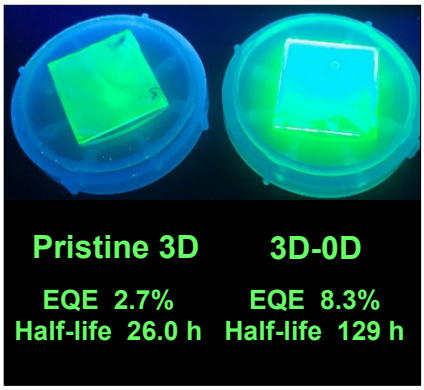

We incorporate highly luminescent 0D Cs_4PbBr_6 nanocrystals into 3D $CsPbBr_3$ films to form single-layer perovskite light-emitting electrochemical cells. The 0D Cs_4PbBr_6 nanocrystals improve the maximum luminance to 11200 cd m^{-2}, the power efficiency to 33.0 Lm W^{-1}, the external quantum efficiency to 8.3%, and the operational stability to 129 h at 10 mA cm^{-2}.